Eur. Phys. J. Spec. Top.
https://doi.org/10.1140/epjs/s11734-025-01707-8

THE EUROPEAN PHYSICAL JOURNAL SPECIAL TOPICS

Review

Cosmic ray energy and composition measurements with GRAPES-3 and other experiments

Fahim Varsi[a]

Institute of Experimental Particle Physics, Karlsruhe Institute of Technology, 76021 Karlsruhe, Germany

Received 15 September 2024 / Accepted 20 May 2025

Abstract Cosmic rays (CRs) are charged nuclei accelerated by natural astrophysical processes to extremely high energies. Despite significant progress in CR research over the past century, their origin and the astrophysical processes responsible for accelerating them to such high energies have yet to be fully understood. A comprehensive understanding requires precise measurement of their energy spectrum and mass composition. This article reviews the CR energy spectrum and mass composition measurements above 100 GeV. The CR energy spectrum is generally described by a power law, with notable spectral features commonly referred to as the knee, ankle, and flux suppression. Direct experiments offer high-precision measurements in the GeV–TeV energy range and have revealed spectral hardening around a few hundred GeV and softening near several tens of TeV in the proton and helium spectra. At energies above hundreds of TeV, CRs are observed by indirect experiments using extensive air showers (EASs). Indirect measurements have also observed further spectral features, such as the hardening in light primaries near hundreds of TeV, the second knee, and the instep. This article highlights the GRAPES-3 experiment, in Ooty, India, focusing on the methodology of using muon multiplicity to estimate mass composition and the observation of spectral hardening at 166 TeV in the CR proton spectrum. These observed spectral features provide important constraints for refining theoretical models of CR origin, acceleration, and propagation. Indirect measurements, particularly of mass composition, are subject to large systematic uncertainties because the interpretation of observables relies on simulations based on hadronic interaction models. This article briefly discusses significant discrepancies in mass composition results arising from the limited theoretical understanding of these models, emphasizing the need for improved hadronic interaction modeling.

1 Introduction

Cosmic rays (CRs) are the most energetic charged particles in the universe, traveling at relativistic speeds, with energies ranging from 10^8 to 10^{20} eV. CRs with energies up to a few hundred TeV can be precisely detected above the atmosphere with direct experiments, such as AMS-02 [1], DAMPE [2], and CALET [3], which employ detectors like magnetic spectrometers and calorimeters aboard satellites or high-altitude balloon flights. However, due to the limited detector exposure and the steeply falling flux of CRs, direct detection of CRs suffers from limited statistics at energies exceeding hundreds of TeV. Consequently, above this energy, CRs are typically observed with large ground-based detector arrays, consisting of either particle detectors or radiation detectors, or a combination of both. These arrays record the extensive air showers (EASs) generated when CRs interact with the atmosphere, thus called indirect observation.

Despite their discovery over a century ago, we lack a comprehensive understanding of fundamental aspects of CRs, such as the identification of their sources and the physical mechanisms responsible for their acceleration and propagation. Nevertheless, precise measurements of the CR energy spectrum, mass composition, and anisotropy in their arrival direction, obtained from both direct and indirect experiments, provide insights into these questions by validating and refining the theoretical models. Figure 1 presents the CR all-particle energy spectrum as measured by several direct and indirect experiments [4–14] over the last 2 decades. These measurements are fairly in agreement when considering their total (statistical and systematic) errors and energy scale uncertainties. The CR energy spectrum exhibits the features called: the knee (at $\sim 4 \times 10^{15}$ eV), the second knee (at $\sim 10^{17}$ eV), the ankle (at

[a] e-mail: fahim.varsi@kit.edu (corresponding author)

Published online: 03 June 2025

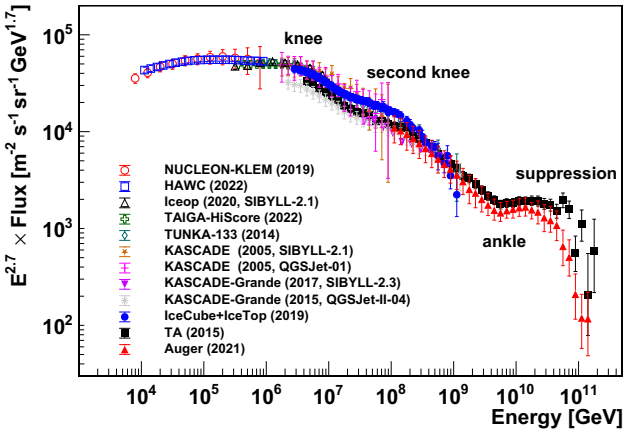

Fig. 1 CR all-particle energy spectrum measured by various direct and indirect experiments [4–14]. The updated cosmic-ray database [15] is used. The error bars represent the total error in the measurements

$\sim 5 \times 10^{18}$ eV), and a flux suppression (at $\sim 5 \times 10^{19}$ eV). These features are believed to be closely connected to the origin, acceleration, and propagation of CRs. However, a comprehensive understanding of their physical implications remains elusive.

These features observed in the all-particle spectrum alone are insufficient for a complete understanding of CRs. A precise estimation of their mass composition is essential, as the interpretation of primary cosmic rays (PCRs) varies across different models or hypotheses concerning their origin, acceleration, and propagation. Direct experiments have good energy and mass resolution, providing precise measurements of the energy spectrum of PCRs. These measurements from different direct experiments are in good agreement and have revealed spectral features in the GeV to TeV energy range.

In contrast, the estimation of mass composition with indirect observations suffers from large systematic uncertainties. These arise not only from inherent fluctuations in EAS development and the limited sampling of large showers but most significantly from the interpretation of the observables that rely on EAS simulations. The first interaction of the EAS development is in a very forward region and governed by soft QCD processes, which lack robust modeling. Moreover, the energies of the first few interactions, for primaries with energies in the PeV range or higher, significantly exceed the maximum energy achievable by current particle accelerators. As a result, in this high-energy regime, interaction models are based on extrapolations tuned with accelerator data, which introduces large uncertainties in the shower observables, including mass-dependent parameters, such as number of muons (N_μ) [16] or depth of shower maximum ($X_{\max}$) [17].

CR composition measurements are important in the TeV to PeV energy range, where direct and indirect measurements overlap. As previously noted, the interpretation of indirect measurements relies heavily on simulations based on the hadronic interaction models, introducing large uncertainties. Lipari illustrates this situation [18], shown in Fig. 2, where CR proton spectra observed by direct and indirect experiments are compared. Lipari only discusses the proton spectra because they constitute a significant fraction of the total CR flux and have been measured with greater accuracy across most of the considered energy range. The CR proton flux observed by various direct experiments shows good agreement and a global fit, represented by a red curve, using a smoothly broken power law (SBPL) with two breaks to capture the hardening and softening of the proton spectra at around 500 GeV and 10 TeV, respectively. The dashed and dash-dotted lines in the figure represent the extrapolation of this global fit to higher energies, connecting direct measurements to those from indirect experiments such as KASCADE [9, 19] and IceTop [12]. However, due to the unavailability of precise CR proton measurements and large uncertainties associated with these indirect observations, an ambiguity in extrapolating the CR proton energy spectrum to higher energies exists.

To resolve this ambiguity, precise composition measurements in the TeV to PeV energy range are essential, with significant overlap with both direct and indirect experiments. The GRAPES-3 [20, 21] is one of such indirect experiments operating in this energy range. It has reported the CR proton spectrum in the energy range of 50 TeV to 1.3 PeV, providing substantial overlap with both direct and indirect measurements. Notably, a spectral hardening at $\sim$ 166 TeV has also been observed, discussed in Sect. 2 in more detail. Furthermore, indirect measurements of the absolute flux of PCRs that rely on hadronic interaction models are valuable when they overlap with direct measurements. This allows the underlying interaction models to be calibrated and checked for validity, thus reducing the uncertainties associated with indirect observations even at higher primary energies.

CRs with energies below the knee are believed to originate within our Galaxy and the knee itself is thought to be associated either with the end of the protons acceleration by the supernova remnants (SNRs) in the Galaxy [22] or with the leakage of protons from the Galaxy [23]. The motion of charged particles in the magnetic field is governed by their magnetic rigidity (R), defined as the ratio of momentum (p) to charge (Ze). Peters [24] first suggested that the maximum energy ($E_{\max}$) achievable by PCRs in a galactic magnetic environment or beyond

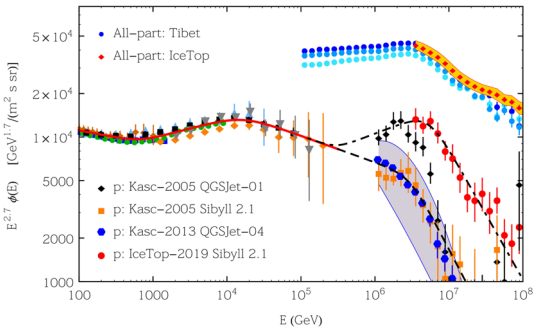

Fig. 2 CR proton energy spectra from direct as well as indirect experiments compiled by P. Lipari [18]. The red line represents the global fit to the direct measurements, and the dashed and dashed-dot lines represent the extrapolation of a global fit to indirect observations at higher energies. This figure is taken from [18]

which they begin to leak from the Galaxy follows a rigidity cutoff, implying that $E_{\max}$ scales proportionally with Ze, meaning heavier nuclei can reach higher energies. Accordingly, the $E_{\max}$ to which an iron primary can be accelerated by galactic SNRs is around 10^{17} eV, which is believed to give rise to the second knee in the all-particle spectrum [22].

Although the positions of the knee and the second knee are in agreement, the observed mass composition and PCR spectra show discrepancies. This requires precise measurements of the mass composition from the knee to the second knee region for a better understanding of the end of CR acceleration by galactic SNRs. Moreover, observations from the Pierre Auger Observatory (PAO) showed that CRs with energies above the ankle are of extragalactic origin [25]. However, the transition from galactic to extragalactic CRs is believed to occur between the knee and the ankle and is still not well understood. The mass composition also plays an important role in several aspects of CRs, including determining the transition between galactic and extra-galactic origins [26], understanding the suppression of the CR flux [27], and estimating the proton-air interaction cross-section at energies beyond the reach man-made particle accelerators [28, 29].

This paper presents a detailed discussion of the CR proton spectrum measurements from GRAPES-3 in the TeV to PeV energy range in Sect. 2. This is followed by some hand-picked measurements from direct and indirect experiments as examples to discuss the current status of the energy spectrum and composition measurements over the entire energy range. In Sect. 3, the spectral features in the CR proton and helium spectra below 100 TeV are discussed with the measurements from CALET. The energy spectrum and mass composition measurements from the IceCube Neutrino Observatory (IceCube) and PAO are discussed in Sect. 4. Finally, Sect. 5 summarizes the main conclusions.

2 CR proton spectrum measured by GRAPES-3

The GRAPES-3 experiment is located in Ooty, India (11.4° N, 76.7° E) at 2200 m above sea level, observing CRs in the several TeV to 10 PeV energy range, with a substantial overlap with direct experiments while covering the knee energy region. It comprises two distinct detector systems: (a) a densely packed array of 400 plastic scintillator detectors, each with a surface area of 1 m^2, spanning an area of 25,000 m^2 [20, 30]. These scintillator detectors sample the charged component of the EAS and record the particle densities and arrival times of EAS secondary particles, which are used to reconstruct arrival direction and shower parameters, including shower size (N_e). (b) a large-area GRAPES-3 muon telescope (G3MT) covering 560 m^2, consisting of sixteen independent muon modules [21]. It shields the electromagnetic and hadronic components of the EAS and provides an energy threshold of 1 GeV $\times$ sec(θ_μ) for muons incident at a zenith angle θ_μ. The muon hits information is utilized to determine the muon multiplicity in the EAS.

The muon multiplicity distribution (MMD) observed by the G3MT is highly sensitive to the mass composition of PCRs. As a result, the observed MMDs are utilized to estimate the relative contributions of proton (H), He, N, Al, and Fe groups without relying on any pre-existing composition models [31]. Gold's iterative unfolding [32] procedure is applied twice in the analysis. In the first step, the unfolding procedure is employed to estimate the relative composition of each PCR group (H, He, N, Al, and Fe) from the observed MMD for each N_e bin. The relative composition of PCRs, as proposed by the GST model [33], is used as the prior distribution, and the optimal stopping iteration for the unfolding process is determined by minimizing the Weighted Mean Square Error (WMSE).

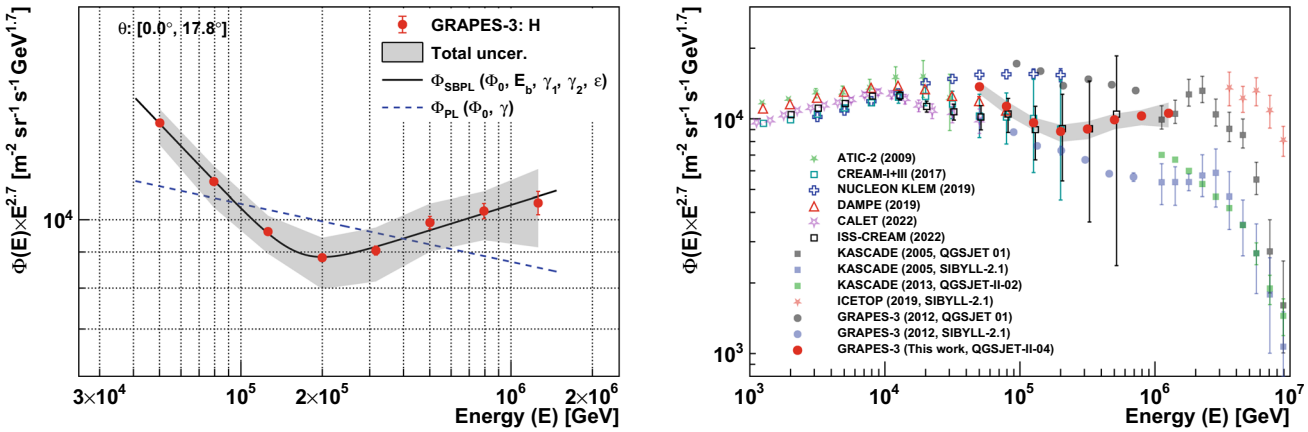

Fig. 3 Left: The differential energy spectrum for the CR proton primary measured with GRAPES-3 [31]. The black solid and blue dashed lines represent the SBPL and PL fitting. Right: The cosmic-ray proton energy spectrum with the GRAPES-3 experiment plotted with data from various direct and indirect experiments [31]

Subsequently, the energy spectrum of the proton primary is unfolded from the corresponding N_e distribution. The N_e distribution for proton primaries is derived by weighting the number of EASs in each bin of the observed N_e distribution with the relative composition of protons obtained from the previous step. Gold's unfolding algorithm is again applied to unfold the proton N_e distribution into the corresponding energy distribution. The optimal stopping iteration is determined based on the criterion of minimizing the WMSE. During the unfolding process, smoothing is applied to the energy distribution after each iteration; however, no smoothing is applied to the energy distribution at the optimal iteration.

The resulting CR proton energy spectrum in the energy range from 50 TeV to 1.3 PeV is presented in the left panel of Fig. 3 [31]. The spectrum shows a spectral hardening at a few hundred TeV and, thus, is modeled using a smoothly broken power law (SBPL), represented by the black curve. The spectral hardening is found to be at 166 ± 8 TeV with spectral indices −3.12 ± 0.02 and −2.56 ± 0.02 before and after the spectral break [31] with a significance of over 3σ deviation from a single power law (PL), represented by the blue dashed line. The observed spectral hardening supports more complex models for galactic CRs, such as ones proposing multiple classes of sources with different rigidity cutoffs [33, 34]. In the right panel of Fig. 3, the measured CR proton energy spectrum is compared with both direct and indirect observations. The flux of the measured proton spectrum shows a good agreement with the results from ISS-CREAM [35] and CREAM I+III [36] at lower energies. At higher energies, the spectrum is consistent with the observations from KASCADE [9] (using the QGSJET-I-01 model).

The High Altitude Water Cherenkov (HAWC), an indirect experiment, has also reported preliminary results on the mass composition of CR proton, helium, and heavy primary groups in the TeV to PeV energy range [37]. These results indicate spectral hardenings at approximately 113 TeV for protons, 104 TeV for helium, and 323 TeV for heavy primary groups. The spectral hardening observed in the CR proton spectrum by HAWC is consistent with the GRAPES-3 results within the total uncertainties.

3 Primary cosmic rays spectra measured by direct experiments

The CR proton and helium energy spectra, as measured by direct experiments, including AMS-02 [38, 39], CREAM-I+III [36], DAMPE [40, 41], and CALET [42, 43] are shown in the left and right panels of Fig. 4, respectively. The observed fluxes from these experiments are fairly consistent with one another within their total uncertainties. The CR proton energy spectra exhibit a spectral hardening near 500 GeV and a spectral softening at approximately 10 TeV. Similarly, the helium spectra exhibit a spectral hardening around 1 TeV and a softening near 35 TeV. These spectral features challenge the single power-law description of the CR flux below the knee and may be explained by the propagation with composite diffusion scenario and contributions from multiple populations of CR sources [44]. In addition, the DAMPE experiment has measured the combined proton and helium spectrum over the energy range from 46 GeV to 316 TeV [45]. By combining the data from both protons and helium primaries, DAMPE improves the statistical significance at higher energies and suggests a spectral hardening around 150 TeV.

In Fig. 5, the proton (top) and helium (bottom) spectra measured by CALET [42, 43] are shown on two different scales: energy per nucleon (left) and magnetic rigidity (right). The positions of spectral breaks, represented by black lines with shaded total uncertainty bands, align when plotted as a function of rigidity rather than energy per nucleon, supporting the hypothesis that the acceleration and propagation of CRs are influenced by the behavior of

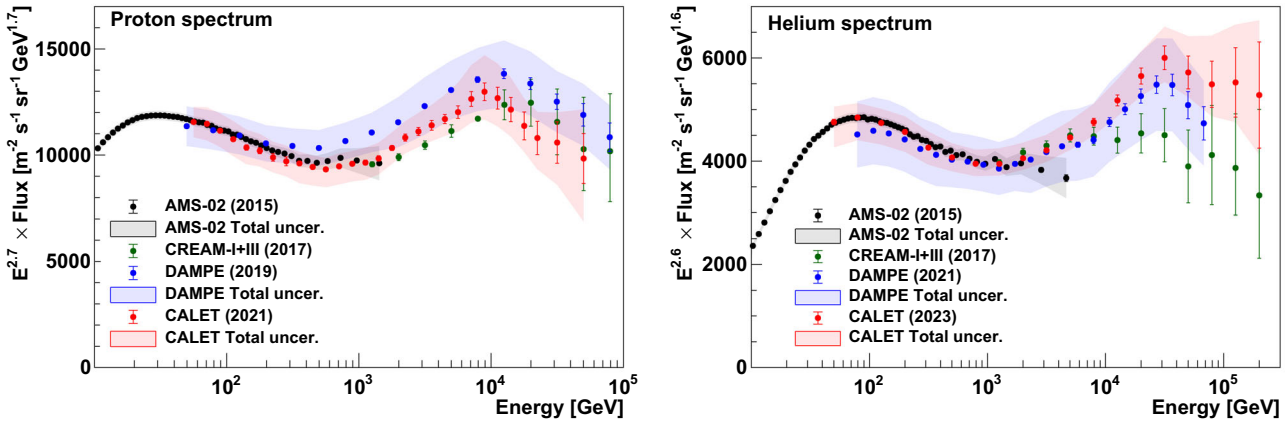

Fig. 4 CR proton (left) and helium (right) energy spectra measured by the AMS-02 [38, 39], CREAM-I+III [36], DAMPE [40, 41], and CALET [42, 43] experiments

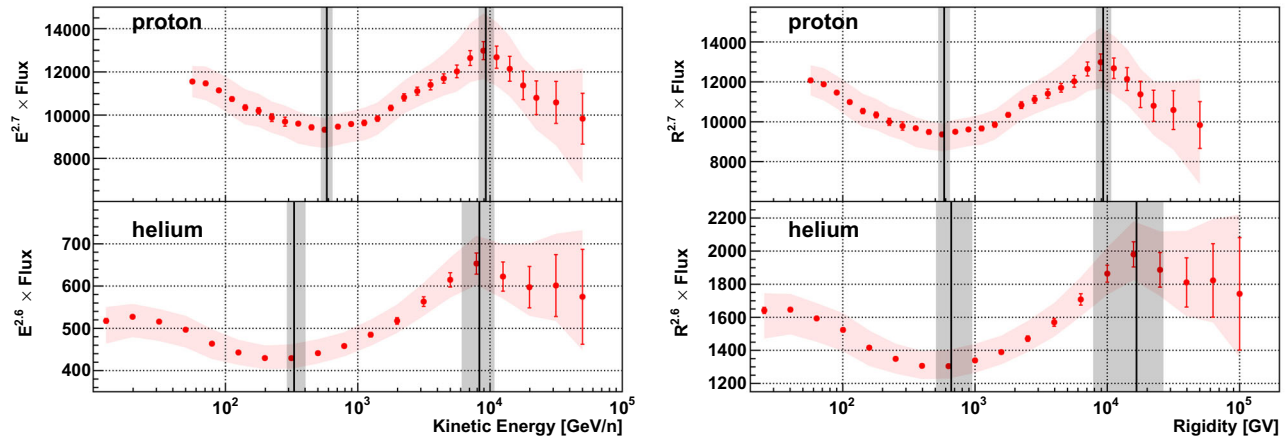

Fig. 5 CR proton (top) and helium (bottom) energy spectra measured by CALET [42, 43] as a function of energy per nucleon (left) and magnetic rigidity (right). Black lines represent the position of the spectral breaks, and the shaded region represents the total uncertainties associated with the measurement of the spectral break

charged particles in magnetic fields [44]. Additionally, the CR proton to helium flux ratio is observed to decrease monotonically, which is yet an unresolved issue. However, one of the hypotheses proposed in [46] suggests that the observed CR proton spectrum may be a combination of two distinct spectra from different types of sources. One class of sources is thought to accelerate all elements uniformly, producing a proton spectrum similar to helium. The other class is either proton-rich or deficient in heavier elements, injecting a proton spectrum with a steeper slope of ≈ 0.3 relative to helium.

4 Energy spectrum and composition measurements at ultra-high energies

In the left panel of Fig. 6, the CR all-particle energy spectrum measured by the IceCube is compared with observations from other experiments [6]. The IceCube spectrum, along with results from other experiments, clearly shows the characteristic knee feature around 4 PeV. Specifically, the TALE measurement is systematically lower than the 3-year IceTop measurement, probably due to uncertainties in energy scale associated with differences in their detection techniques. Due to the steepening of the spectrum above the knee, such uncertainties have an amplified impact on the measured flux. This panel also includes the all-particle spectrum measured by the HAWC experiment [47] in the energy range from 10 TeV to 500 TeV, which exhibits a spectral softening at approximately 45 TeV. The right panel of Fig. 6 presents the all-particle energy spectrum for energies above 100 PeV as measured by the PAO [14]. In addition to the well-known features, ankle at 4.9×10^{18} eV and flux suppression at $\sim$

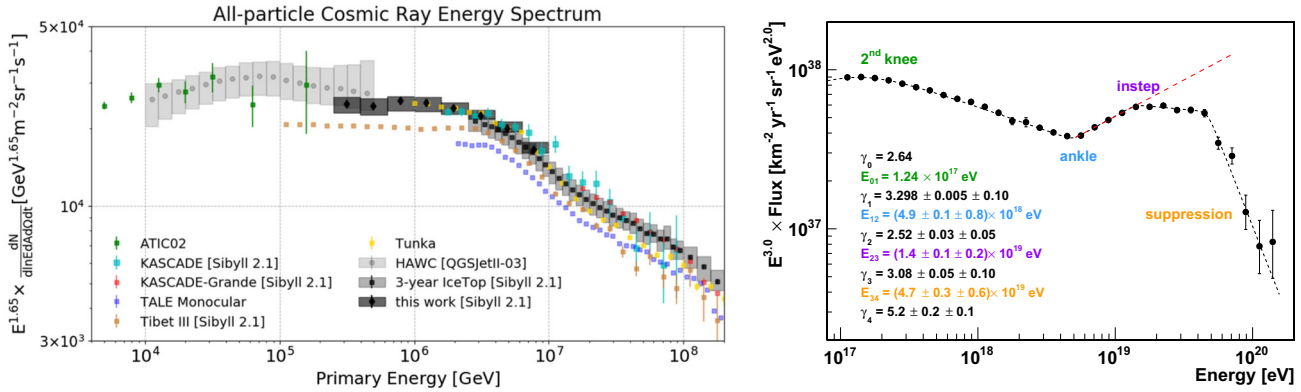

Fig. 6 Left: The CR all-particle spectrum measured by IceCube compared with observations from indirect experiments. This figure is taken from [6]. Right: The CR all-particle spectrum measured by the PAO [14] in the energy range above 100 PeV

4.7×10^{19} eV, additional spectral features are observed at higher energies. These features include the second knee at 1.24×10^{17} eV and a feature referred to as the 'instep' near $\sim 1.4 \times 10^{19}$ eV.

HAWC has reported [48] that the spectral softening at around 45 TeV arises from the superposition of the spectra of PCRs, each exhibiting the spectral softening features near tens of TeV. As previously mentioned, the knee (the second knee) in the CR all-particle spectrum is believed to signify either the maximum energy to which CR proton (iron) can be accelerated by the galactic SNRs [22] or start of their escape from the Galaxy [23]. Measurements from KASCADE [9, 19] and IceTop [12] support the rigidity-dependent cutoff in PCR spectra, as a result, the all particle spectrum becomes heavier in the energy range from the knee to the second knee.

Recently, the PAO reported measurements of the $X_{\max}$ over the energy range from 1 EeV to 100 EeV, using the water Cherenkov surface detectors (SD) and fluorescent detectors (FD) [49], as shown in the top panel of Fig. 7. The energy evolution of the $X_{\max}$ is described using the elongation rate model, represented by the red line. The elongation rate refers to the rate of change of the $X_{\max}$ with respect to the primary energy. The analysis reveals three significant spectral breaks at 6.5 EeV, 11 EeV, and 31 EeV, with the total uncertainties associated with these breaks represented by the gray band. These break points are consistent with the ankle, the instep, and

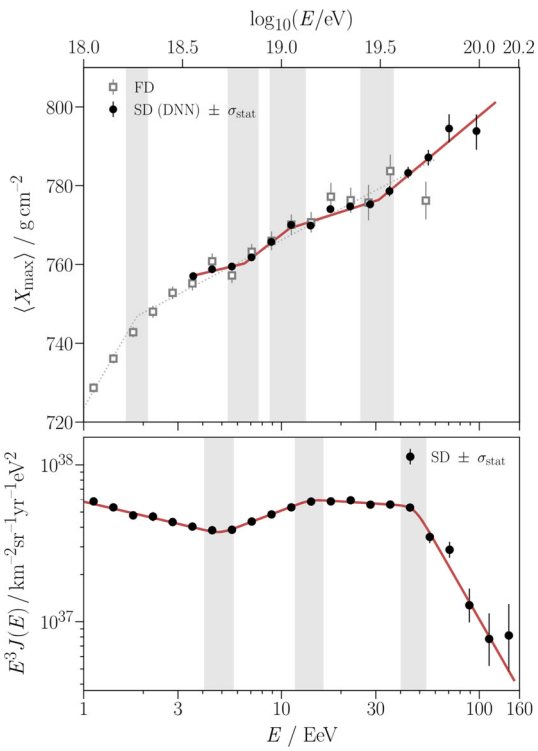

Fig. 7 Measurements by PAO [49]. Top: $X_{\max}$ using SD (solid dots) and FD (open squares). The red and dotted gray lines represent the elongation model. Bottom: The CR all-particle energy spectrum measured using SD. The gray areas represent the uncertainties in the spectral breaks

the suppression features observed in the all-particle energy spectrum, as shown in the bottom panel of Fig. 7, considering the total uncertainties of these features, also indicated by gray bands. Similar spectral breaks are suggested in [27], where an astrophysical model with two extragalactic source populations is employed to describe the ankle region. Furthermore, the mass composition is reported to become increasingly heavier with increasing energy and shows incompatibility with a major contribution from light nuclei in the energy range between 50 and 100 EeV. Consequently, these observations do not support models attributing the flux suppression to the interaction of protons with the cosmic microwave background.

As already mentioned, the interpretation of indirect observations in CR studies relies on hadronic interaction models, introducing significant uncertainties in the mass composition estimation. This is illustrated in Fig. 8, where the mean logarithmic mass ($\langle \ln A \rangle$), derived from $X_{\max}$ measurements by the PAO, is shown for three different hadronic interaction models: QGSJet-II-04, EPOS-LHC, and Sibyll 2.3c, alongside results from other experiments [50]. A substantial difference in results from TALE, Tunka-133, and Yakutsk indicates the presence of unaccounted systematic uncertainties in some of these experiments. In addition, for the PAO, large model-dependent systematic differences are evident in the $\langle \ln A \rangle$ values. These inconsistencies arise from the lack of sufficient theoretical understanding of soft QCD processes, which govern the forward region of hadronic interactions. As a result, current models do not fully describe the data, leading to different mass composition results for different models. Thus, the precise CR mass composition by indirect observations necessitates better modeling of the hadronic interactions, particularly at high energies.

5 Conclusion

Both direct and indirect measurements have advanced our understanding of the CR energy spectrum and mass composition. Direct experiments have revealed complex features, such as spectral hardening near hundreds of GeV and softening around tens of TeV in proton and helium spectra. The GRAPES-3 experiment has observed a spectral hardening at 166 TeV in the CR proton spectrum. In addition to the well-known spectral features like the knee, the ankle, and the flux suppression, indirect observations have identified additional features such as the second knee and the instep beyond PeV energies. These spectral features support the need for more sophisticated models concerning the CR origin, acceleration, and propagation.

As discussed, mass composition measurements play a crucial role in understanding various aspects of CRs. However, one of the major challenges in obtaining precise mass composition measurements by indirect experiments is the limited theoretical understanding of soft QCD processes, governing the first interaction of the EAS development. This limited knowledge introduces significant uncertainties in producing secondary particle and their lateral and longitudinal distribution. These uncertainties propagate to the mass-dependent observables, resulting in inconsistencies across experiments that use different mass-dependent observables and detection techniques. Furthermore, extrapolation of different hadronic interaction models to higher energies leads to large uncertainties, even within the same experiment, depending on the models used.

Another significant challenge in CR mass composition measurements is the limited resolution of the mass-dependent observables, especially for heavier primaries, due to the inherent shower-to-shower fluctuations. To improve this resolution, major existing observatories such as IceCube and PAO, have planned or ongoing upgrades.

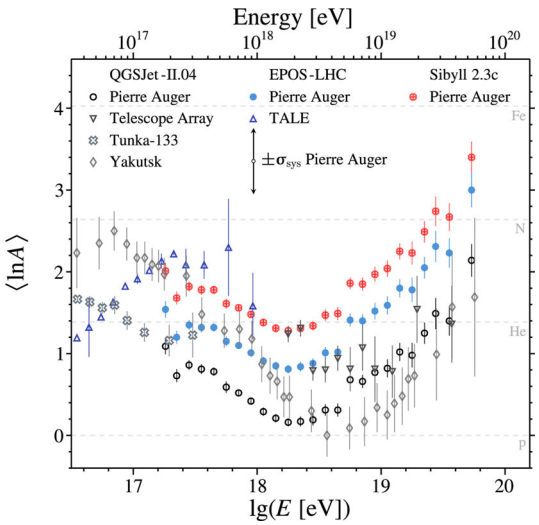

Fig. 8 The mean logarithmic mass of CR obtained from the $X_{\max}$ data observed by different experiments for different hadronic interaction models. The figure is taken from [50]

The IceCube is planned to upgrade to IceCube-Gen2, This upgrade will expand the existing IceCube by adding an $8\,km^3$ in-ice array, a $\sim 6\,km^2$ surface array of hybrid scintillator and radio antenna detectors, and a $\sim 500\,km^2$ radio array. The PAO has upgraded to AugerPrime, where each SD station is upgraded with a scintillator detector on top, a radio antenna, and an underground muon detector. These upgrades improve the form factor, defined as the difference in the mean of mass-dependent observables for proton and iron in the unit of their combined spread, to better than 2.0 for both IceCube-Gen2 and AugerPrime. Furthermore, multi-hybrid detection allows for simultaneous measurement of various observables, which can help tune and test interaction models. In addition, next-generation experiments, such as the Probe of MultiMessenger Astrophysics (POEMMA) space-based observatory, the Giant Radio Array for Neutrino Detection (GRAND) ground array, and the Global Cosmic Ray Observatory (GCOS) ground array, are expected to provide high-precision complementary information at the ultra-high energies and the Square Kilometer Array (SKA) at the high energies. These upcoming efforts are critical to advancing the understanding of the CRs above tens of PeV energies.

Acknowledgements I would like to express my sincere gratitude to the reviewers for their time and effort in reviewing the manuscript. I sincerely appreciate valuable comments and suggestions from the reviewers and Andreas Haungs, which helped me to improve the quality of the manuscript.

Funding Open Access funding enabled and organized by Projekt DEAL.

Data availability There is no new datasets were generated or analyzed for this manuscript. The data for various plots are available in their respected refereces mention in the manuscipt.

References

1. M. Aguilar et al., The Alpha Magnetic Spectrometer (AMS) on the international space station: part II—results from the first seven years. Phys. Rep. **894**, 1 (2021). https://doi.org/10.1016/j.physrep.2020.09.003
2. J. Chang et al., The DArk Matter Particle Explorer mission. Astropart. Phys. **95**, 6 (2017). https://doi.org/10.1016/j.astropartphys.2017.08.005
3. P.S. Marrocchesi, CALET on the ISS: a high energy astroparticle physics experiment. J. Phys. Conf. Ser. **718**, 052023 (2016). https://doi.org/10.1088/1742-6596/718/5/052023/pdf
4. V. Grebenyuk et al., Energy spectra of abundant cosmic-ray nuclei in the NUCLEON experiment. Adv. Sp. Res. **64**, 2546 (2019). https://doi.org/10.1016/j.asr.2019.10.004
5. J.A. Morales-Soto et al., The all-particle cosmic ray energy spectrum measured with HAWC. In: Proc. Sci., ICRC2021, 330 (2021). https://doi.org/10.22323/1.395.0330
6. M.G. Aartsen et al., Cosmic ray spectrum from 250 TeV to 10 PeV using IceTop. Phys. Rev. D **102**, 122001 (2020). https://doi.org/10.1103/PhysRevD.102.122001
7. I.I. Astapov et al., Cosmic-Ray research at the TAIGA astrophysical facility: results and plans. J. Exp. Theor. Phys. **134**, 469 (2022). https://doi.org/10.1134/S1063776122040136
8. V.V. Prosin et al., Tunka-133: results of 3 year operation. Nucl. Instrum. Methods A **756**, 94 (2014). https://doi.org/10.1016/j.nima.2013.09.018
9. T. Antoni et al., KASCADE measurements of energy spectra for elemental groups of cosmic rays: results and open problems. Astropart. Phys. **24**, 1 (2005). https://doi.org/10.1016/j.astropartphys.2005.04.001
10. S. Schoo et al., The energy spectrum of cosmic rays in the range from 10^{14} to 10^{18} eV. In: Proc. Sci., ICRC2015, 263 (2015). https://doi.org/10.22323/1.236.0263
11. J.C. Arteaga-Velázquez et al., Measurements of the muon content of EAS in KASCADE-Grande compared with SIBYLL 2.3 predictions. In: Proc. Sci., ICRC2017, 316 (2017). https://doi.org/10.22323/1.301.0316
12. M.G. Aartsen et al., Cosmic ray spectrum and composition from PeV to EeV using 3 years of data from IceTop and IceCube. Phys. Rev. D **100**, 082002 (2019). https://doi.org/10.1103/PhysRevD.100.082002
13. D. Ivanov, TA spectrum summary. In: Proc. Sci., ICRC2015, 349 (2015). https://doi.org/10.22323/1.236.0349
14. P. Abreu et al., The energy spectrum of cosmic rays beyond the turn-down around 10^{17} eV as measured with the surface detector of the Pierre Auger Observatory. Eur. Phys. J. C **81**, 966 (2021). https://doi.org/10.1140/epjc/s10052-021-09700-w

15. D. Maurin et al., A cosmic-ray database update: CRDB v4.1. Eur. Phys. J. C **83**, 971 (2023). https://doi.org/10.1140/epjc/s10052-023-12092-8
16. J. Albrecht et al., The Muon Puzzle in cosmic-ray induced air showers and its connection to the Large Hadron Collider. Astrophys. Sp. Sci. **367**, 27 (2022). https://doi.org/10.1007/s10509-022-04054-5
17. A. Abdul Halim et al., Measurement of the depth of maximum of air-shower profiles with energies between $10^{18.5}$ and 10^{20} eV using the surface detector of the Pierre Auger Observatory and deep learning. Phys. Rev. D **111**, 022003 (2025). https://doi.org/10.1103/PhysRevD.111.022003
18. P. Lipari, S. Vernetto, The shape of the cosmic ray proton spectrum. Astropart. Phys. **120**, 102441 (2020). https://doi.org/10.1016/j.astropartphys.2020.102441
19. W.D. Apel et al., KASCADE-Grande measurements of energy spectra for elemental groups of cosmic rays. Astropart. Phys. **47**, 54 (2013). https://doi.org/10.1016/j.astropartphys.2013.06.004
20. S.K. Gupta et al., GRAPES-3-A high-density air shower array for studies on the structure in the cosmic-ray energy spectrum near the knee. Nucl. Instrum. Methods A **540**, 311 (2005). https://www.sciencedirect.com/science/article/pii/S016890020402426X
21. Y. Hayashi et al., A large area muon tracking detector for ultra-high energy cosmic ray astrophysics-the GRAPES-3 experiment. Nucl. Instrum. Methods Phys. A **545**, 643 (2005). https://www.sciencedirect.com/science/article/pii/S0168900205007643
22. P. Blasi, The origin of galactic cosmic rays. Astron. Astrophys. Rev. **21**, 70 (2013). https://doi.org/10.1007/s00159-013-0070-7
23. G. Giacinti, M. Kachelriess, D.V. Semikoz, Explaining the spectra of cosmic ray groups above the knee by escape from the Galaxy. Phys. Rev. D **90**, 041302(R) (2014). https://doi.org/10.1103/PhysRevD.90.041302
24. B. Peters, Primary cosmic radiation and extensive air showers. Il Nuovo Cimento (1955-1965) **22**, 800 (1961)
25. A. Aab et al., Observation of a large-scale anisotropy in the arrival directions of cosmic rays above 8×10^{18} eV. Science **357**, 1266 (2017). https://doi.org/10.1126/science.aan4338
26. R. Aloisio, V. Berezinsky, A. Gazizov, Transition from galactic to extragalactic cosmic rays. Astropart. Phys. **39**, 129 (2012). https://doi.org/10.1016/j.astropartphys.2012.09.007
27. A. Abdul Halim et al., Constraining the sources of ultra-high-energy cosmic rays across and above the ankle with the spectrum and composition data measured at the Pierre Auger Observatory. J. Cosmo. Astropart. Phys. **05**, 024 (2023). https://doi.org/10.1088/1475-7516/2023/05/024
28. P. Abreu et al., Measurement of the proton-air cross section at $\sqrt{s} = 57$ TeV with the Pierre Auger observatory. Phys. Rev. Lett. **109**, 062002 (2012). https://doi.org/10.1103/PhysRevLett.109.062002
29. P. Lipari, Spectra and composition of ultrahigh-energy cosmic rays and the measurement of the proton-air cross section. Phys. Rev. D **103**, 103009 (2021). https://doi.org/10.1103/PhysRevD.90.041302
30. P.K. Mohanty et al., Measurement of some EAS properties using new scintillator detectors developed for the GRAPES-3 experiment. Astropart. Phys. **31**, 24 (2009). https://doi.org/10.1016/j.astropartphys.2008.11.004
31. F. Varsi et al., Evidence of a hardening in the cosmic ray proton spectrum at around 166 TeV observed by the GRAPES-3 experiment. Phys. Rev. Lett. **132**, 051002 (2024). https://doi.org/10.1103/PhysRevLett.132.051002
32. R. Gold, An iterative unfolding method for response matrices, Argonne National Laboratory, USA, Rep. ANL-6984, (1964) https://doi.org/10.2172/4634295
33. T.K. Gaisser, T. Stanev, S. Tilav, Cosmic ray energy spectrum from measurements of air showers. Front. Phys. **8**, 748 (2013). https://doi.org/10.1007/s11467-013-0319-7
34. V.I. Zatsepin, N.V. Sokolskaya, Three component model of cosmic ray spectra from 10 GeV to 100 PeV. Astron. Astrophys. **458**, 1 (2006). https://doi.org/10.1051/0004-6361:20065108
35. G.H. Choi et al., Measurement of high-energy cosmic-ray proton spectrum from the ISS-CREAM experiment. Astrophys. J. **940**, 107 (2022). https://doi.org/10.3847/1538-4357/ac9d2c
36. Y.S. Yoon et al., Proton and helium spectra from the CREAM-III flight. Astrophys. J. **839**, 5 (2017). https://doi.org/10.3847/1538-4357/aa68e4/meta
37. J.C. Arteaga Velazquez et al., Analysis of the composition of TeV cosmic rays with HAWC. In: Proc. Sci., ICRC2023, 299 (2023). https://pos.sissa.it/444/299/
38. M. Aguilar et al., Precision measurement of the proton flux in primary cosmic rays from rigidity 1 GV to 1.8 TV with the alpha magnetic spectrometer on the International Space Station. Phys. Rev. Lett. **114**, 171103 (2015). https://doi.org/10.1103/PhysRevLett.114.171103
39. M. Aguilar et al., Precision measurement of the helium flux in primary cosmic rays of rigidities 1.9 GV to 3 TV with the alpha magnetic spectrometer on the International Space Station. Phys. Rev. Lett. **115**, 211101 (2015). https://doi.org/10.1103/PhysRevLett.115.211101
40. Q. An et al., Measurement of the cosmic ray proton spectrum from 40 GeV to 100 TeV with the DAMPE satellite. Sci. Adv. **5**, eaax3793 (2019). https://doi.org/10.1126/sciadv.aax3793
41. F. Alemanno et al., Measurement of the cosmic ray helium energy spectrum from 70 GeV to 80 TeV with the DAMPE space mission. Phys. Rev. Lett. **126**, 201102 (2021). https://doi.org/10.1103/PhysRevLett.126.201102
42. O. Adriani et al., Observation of spectral structures in the flux of cosmic-ray protons from 50 GeV to 60 TeV with the calorimetric electron telescope on the International Space Station. Phys. Rev. Lett. **129**, 101102 (2022). https://doi.org/10.1103/PhysRevLett.129.101102

43. O. Adriani et al., Direct measurement of the cosmic-ray helium spectrum from 40 GeV to 250 TeV with the calorimetric electron telescope on the International Space Station. Phys. Rev. Lett. **130**, 171002 (2023). https://doi.org/10.1103/PhysRevLett.130.171002
44. S. Recchia, S. Gabici, Origin of the spectral features observed in the cosmic-ray spectrum. Astron. Astrophys. **692**, A20 (2024). https://doi.org/10.1051/0004-6361/202349005
45. F. Alemanno et al., Measurement of the cosmic p+He energy spectrum from 46 GeV to 316 TeV with the DAMPE space mission, arXiv:2304.00137v4 (2023)
46. I.V. Moskalenko, Direct measurements of cosmic rays and their possible interpretations. In: Proc. Sci., ICRC2023, 020 (2023). https://doi.org/10.22323/1.444.0020
47. R. Alfaro et al., All-particle cosmic ray energy spectrum measured by the HAWC experiment from 10 to 500 TeV. Phys. Rev. D **96**, 122001 (2017). https://doi.org/10.1103/PhysRevD.96.122001
48. J.C. Arteaga Velazquez et al., HAWC measurements of the energy spectra of cosmic ray protons, helium and heavy nuclei in the TeV range, Proc. Sci., ICRC2021, 374 (2021). https://doi.org/10.22323/1.395.0374
49. A. Abdul Halim et al., Inference of the mass composition of cosmic rays with energies from $10^{18.5}$ to 10^{20} eV using the Pierre Auger observatory and deep learning. Phys. Rev. Lett. **134**, 021001 (2025). https://doi.org/10.1103/PhysRevLett.134.021001
50. A. Coleman et al., Ultra high energy cosmic rays The intersection of the Cosmic and Energy Frontiers. Astropart. Phys. **149**, 102819 (2023). https://doi.org/10.1016/j.astropartphys.2023.102819